

## Article

# Pressure Tuned Structural, Electronic and Elastic Properties of $U_3Si_2C_2$ : A First Principles Study

Moran Bu <sup>1,2</sup>, Yaolin Guo <sup>1,\*</sup>, Diwei Shi <sup>1</sup>, Zhen Liu <sup>3</sup>, Jiexi Song <sup>1,4</sup>, Yifan Li <sup>1,3</sup>, Erxiao Wu <sup>1,2</sup>, Xinyu Chen <sup>5</sup>, Yanqing Qin <sup>4</sup>, Yang Yang <sup>6,\*</sup>  and Shiyu Du <sup>1,3,\*</sup>

<sup>1</sup> Engineering Laboratory of Advanced Energy Materials, Ningbo Institute of Materials Technology and Engineering, Chinese Academy of Sciences, Ningbo 315201, China; bumoran19@mailsucas.ac.cn (M.B.); shidw1@shanghaitech.edu.cn (D.S.); songjiexi@mail.nwpu.edu.cn (J.S.); liyifan@nimte.ac.cn (Y.L.); wuerxiao@nimte.ac.cn (E.W.)

<sup>2</sup> College of Materials Sciences and Opto-Electronic Technology, University of Chinese Academy of Sciences, 19A Yuquan Rd., Shijingshan District, Beijing 100049, China

<sup>3</sup> College of Materials Science and Chemical Engineering, Harbin Engineering University, Harbin 150001, China; liuzhen@nimte.ac.cn

<sup>4</sup> Department of Applied Physics, Northwestern Polytechnical University, Xi'an 710072, China; thblsdx@mail.ustc.edu.cn

<sup>5</sup> Institute of Chemicobiology and Functional Materials, School of Chemical Engineering, Nanjing University of Science and Technology, Nanjing 210094, China; chenxinyu@njjust.edu.cn

<sup>6</sup> State Key Laboratory for Mechanical Behavior of Materials, Xi'an Jiaotong University, Xi'an 710049, China

\* Correspondence: guoyaolin@nimte.ac.cn (Y.G.); yangymse@xjtu.edu.cn (Y.Y.); dushiyu@nimte.ac.cn (S.D.)



**Citation:** Bu, M.; Guo, Y.; Shi, D.; Liu, Z.; Song, J.; Li, Y.; Wu, E.; Chen, X.; Qin, Y.; Yang, Y.; et al. Pressure Tuned Structural, Electronic and Elastic Properties of  $U_3Si_2C_2$ : A First Principles Study. *Crystals* **2021**, *11*, 1420. <https://doi.org/10.3390/cryst11111420>

Academic Editor: Claudio Cazorla

Received: 1 November 2021

Accepted: 18 November 2021

Published: 20 November 2021

**Publisher's Note:** MDPI stays neutral with regard to jurisdictional claims in published maps and institutional affiliations.



**Copyright:** © 2021 by the authors. Licensee MDPI, Basel, Switzerland. This article is an open access article distributed under the terms and conditions of the Creative Commons Attribution (CC BY) license (<https://creativecommons.org/licenses/by/4.0/>).

**Abstract:**  $U_3Si_2C_2$  is expected to be a new nuclear fuel as a ternary compound of uranium, silicon and carbon. However, the relevant research on  $U_3Si_2C_2$  under accident conditions is rarely reported. Hence it is necessary to explore the service behavior of the potential U-Si-C ternary nuclear fuel in extreme environments. In this work, the structural characteristics, electronic behaviors and mechanical properties of  $U_3Si_2C_2$ , such as stable crystalline structures, density of states, charge distributions, electron localization function, electronic thermal conductivity and elastic modulus under extreme high pressure are calculated by density functional theory. The calculation results show that the lattice volume sharply increases when the external stress reached 9.8 GPa. Ionic and metallic nature coexist as to the bonding characteristics of  $U_3Si_2C_2$ , and the ionic takes the dominant position in bonding. The toughness of  $U_3Si_2C_2$  is predicted to be better compared to  $U_3Si_2$ . Our theoretical investigation may help with the application of  $U_3Si_2C_2$ -based fuel and the design of ternary uranium fuels.

**Keywords:** accident tolerant fuel;  $U_3Si_2C_2$ ; density functional theory; high pressure behavior

## 1. Introduction

Since the Fukushima nuclear accident, the safety of fuel pellet in working and accident conditions has been paid increasing attention. The accident tolerant fuel systems (ATFs) have become a major concern of nuclear material research, attributing to its abilities of tolerance for the extreme working and accident conditions (high temperature, extreme pressure, irradiation, etc.). Considering the low thermal conductivity of traditional  $UO_2$  fuel, developing new materials with higher thermal conductivity and other advantageous properties to replace  $UO_2$  has aroused researcher's interest [1]. A lot of Uranium-based binary compounds/alloys have been treated as alternative to uranium dioxide, because of their thermo-physical properties, such as uranium silicide ( $USi_3$ ,  $USi_2$ ,  $U_3Si_5$ ,  $USi$ ,  $U_3Si_2$ , and  $U_3Si$ ) [2–8], uranium nitride ( $UN$ ,  $UN_2$ , and  $U_4N_7$ ) [3,9] and uranium carbide ( $UC$ ,  $UC_2$ , and  $U_2C_3$ ) [10–13]. Contemplating the disabilities of these binary compounds, such as the terrible mechanical behavior of  $U_3Si_2$ , ternary uranium compounds has also been researched, such as U-Si-Mo [14–16], U-Al-Zr [17], and U-Si-Al [17–20]. Recently,  $U_3Si_2C_2$

becomes potential candidate fuel due to its excellent stability, radiation, and oxidation resistance and high thermal conductivity [21,22]. Pressure is an important variable for nuclear fuel systems because of the local extreme pressure (in the GPa range) environment appearing in working conditions (such as near the fission gas bubbles [23]), and the pressure may cause the transformations of electronic and crystalline structures [24,25]. However, little is yet known on its evolution behavior under extreme pressure environment.

The ternary system uranium–silicon–carbon (U-Si-C) is of certain interest for nuclear energy on account of the neutron transparency of carbon and silicon [26]. Some experimental and theoretical researches on uranium-silicon-carbon ternary compounds have been carried out since 1960s. Smith et al. [27] found two unidentified phases above 1700 °C by studying the high temperature behavior of UC-SiC and UC<sub>2</sub>-SiC systems. Blum et al. [28,29] and Pöttgen et al. [30] found that these two undefined phases were U<sub>3</sub>Si<sub>2</sub>C<sub>2</sub> and U<sub>20</sub>Si<sub>16</sub>C<sub>3</sub>. Pöttgen et al. [30] also measured the magnetic susceptibility and electrical conductivity of U<sub>3</sub>Si<sub>2</sub>C<sub>2</sub>, which belongs to I4/mmm space group. Matar and Pöttgen [31] calculated the electronic structure and chemical bonding of U<sub>3</sub>Si<sub>2</sub>C<sub>2</sub> based on density functional theory (DFT) and they found that uranium selectively bonds with Si and C. Some new methods for preparing U<sub>3</sub>Si<sub>2</sub>C<sub>2</sub> fuel pallet have been developed by Yang et al. [21,22], and they claimed this imitated MAX phase material have high thermal conductivity at high temperature, excellent radiation and oxidation resistance, which are favorable for nuclear fuel performance.

The high pressure behaviors of U-C [32–34] and U-Si [35,36] compounds have also been studied to evaluate their structural stabilities. The high-pressure behavior of UC<sub>2</sub> shows tetragonal → monoclinic → orthorhombic transition for this material with transition pressures of 8 GPa and 42 GPa [34]. Guo et al. researched the pressure dependence of the crystal structure of U<sub>3</sub>Si<sub>2</sub> using high-energy synchrotron X-ray diffraction coupled with Rietveld analysis and obtained its a- and c-axial moduli as well as bulk modulus [35]. However, there is almost no public report on the high-pressure evolution of U-Si-C compounds. In this work, the high-pressure electronic and structural evolutions of U<sub>3</sub>Si<sub>2</sub>C<sub>2</sub> are performed through density functional theory (DFT) calculations to characterize the structural and mechanical stabilities.

## 2. Methodology

The DFT theoretical calculations in this paper are carried out using Vienna ab initio simulations package (VASP) [37,38]. During the calculation process, the projected-augmented-wave potential (PAW) [39] is adopted with the cutoff energy of 520 eV. The scheme by Perdew–Burke–Ernzerhof (PBE) [40] is functional with generalized gradient approximation (GGA) can be used to describe the exchange and correlation interactions between electrons. The strong on-site Coulomb interaction among the localized U 5f electrons is eliminated by Hubbard *U* approximation (GGA + *U*) [41], which has been proved effective in our previous works on U-Si and U-Si-Al compounds [19,20,42]. A 8 × 8 × 4  $\gamma$ -centered Monkhorst–Pack [43] k-point grid is adopted for the unit cell for Brillouin zone sampling. The optimizations of the structural parameters under different pressures from 0 to 24 GPa are performed through conjugate-gradient algorithm [44] in the condition that the force on the atoms is less than 0.001 eV/Å and the total energy difference is smaller than 1.0 × 10<sup>−6</sup> eV/cell. The theoretical phonon spectrum is obtained according to the density functional perturbation theory (DFPT) [45,46] with 2 × 2 × 1 supercell, and the phonon band structures are calculated by the Phonopy package [47]. The ab-initio molecular dynamics (AIMD) simulations for 56-atom supercell under NPT ensemble from 300 to 2100 K with a time step of 1 fs can be employed to determine the structural stability under extreme temperatures.

The mechanical anisotropy is evaluated by universal anisotropic index  $A^U$  [48] in this work, which is described as Equation (1):

$$A^U = 5 \frac{G^V}{G^R} + \frac{B^V}{B^R} - 6 \quad (1)$$

For crystals with tetragonal symmetry, [49–51], the  $B^V$  and  $B^R$  are the bulk modulus following Voigt and Reuss approximations respectively,  $G^V$  and  $G^R$  are the corresponding shear modulus. These four variables can be expressed as Equations (2)–(7):

$$B^V = [2(C_{11} + C_{12}) + 4C_{13} + C_{33}]/9 \quad (2)$$

$$G^V = (M + 3C_{11} - 3C_{12} + 12C_{44} + 6C_{66})/30 \quad (3)$$

$$B^R = C^2/M \quad (4)$$

$$G^R = 15/[ (18B^V)/C^2 + 6/(C_{11} - C_{12}) + 6/C_{44} + 3/C_{66} ] \quad (5)$$

$$B^R = C^2/M \quad (6)$$

$$M = C_{11} + C_{12} + 2C_{33} - 4C_{13} \quad (7)$$

In which  $S_{ij}$  represents the elastic compliance constants, and  $C_{ij}$  is the elastic constants.

The mechanical anisotropy is also evaluated by three-dimensional (3D) Young's modulus. The directional dependent Young's moduli for tetragonal crystal system can be calculated by Equation (8):

$$\frac{1}{E_t} = l_1^4 S_{11} + l_2^4 S_{11} + 2l_1^2 l_2^2 S_{12} + 2l_1^2 l_3^2 S_{13} + 2l_2^2 l_3^2 S_{13} + l_3^4 S_{33} + l_1^2 l_3^2 S_{44} + l_2^2 l_3^2 S_{44} + l_1^2 l_2^2 S_{66} \quad (8)$$

$l_1$ ,  $l_2$ , and  $l_3$  donate the cosines between the given vector and a, b, and c axis. In the tetragonal crystal, 6 independent compliance constants  $S_{ij}$  are available.

The Young's modulus  $E$  and Poisson's ratio  $\nu$  [49] are expressed as follows:

$$E = \frac{9BG}{3B + G} \quad (9)$$

$$\nu = \frac{3B - 2G}{2(3B + G)} \quad (10)$$

### 3. Results and Discussions

#### 3.1. Ground State Structural Parameters

The original structure of  $U_3Si_2C_2$  is obtained from Pöttgen et al. [18]. The  $U_3Si_2C_2$  compound crystallizes in the structure of tetragonal, belonging to the space group of  $I4/mmm$ , which has 14 atoms in the conventional unit cell and an exact 3:2:2 stoichiometry, as shown in Figure 1. The types of uranium atoms can be divided into two (U1 and U2) [19] by their nearest neighbor atoms. The structural optimization of  $U_3Si_2C_2$  are implemented with GGA and GGA +  $U$  methods, respectively. In order to study the ground-state properties of  $U_3Si_2C_2$ , the common DFT +  $U$  method is adopted for structural optimization, which has been widely used for other nuclear fuels such as  $UO_2$  [52], U-Si [36,42], and U-C [32,53]. The influence of Hubbard  $U$  parameter values from 0 to 4 eV on the lattice constants (a and c) and the volumes (V) of  $U_3Si_2C_2$  unit cells are listed in Table 1. The values of a, c and V calculated by using PAW-GGA potential are 3.645 Å, 16.790 Å, and 222.24 Å<sup>3</sup>. The volume obtained from PAW-GGA potential underestimates severely compared with the experimental [30] and DFT +  $U$  [31] results. However, as shown in Table 1, the optimized volume using GGA +  $U$  ( $U = 3.5$  eV) is in better agreement with the experimental data. Therefore, 3.5 eV is chosen as the calculation parameter of  $U$  in following studies.

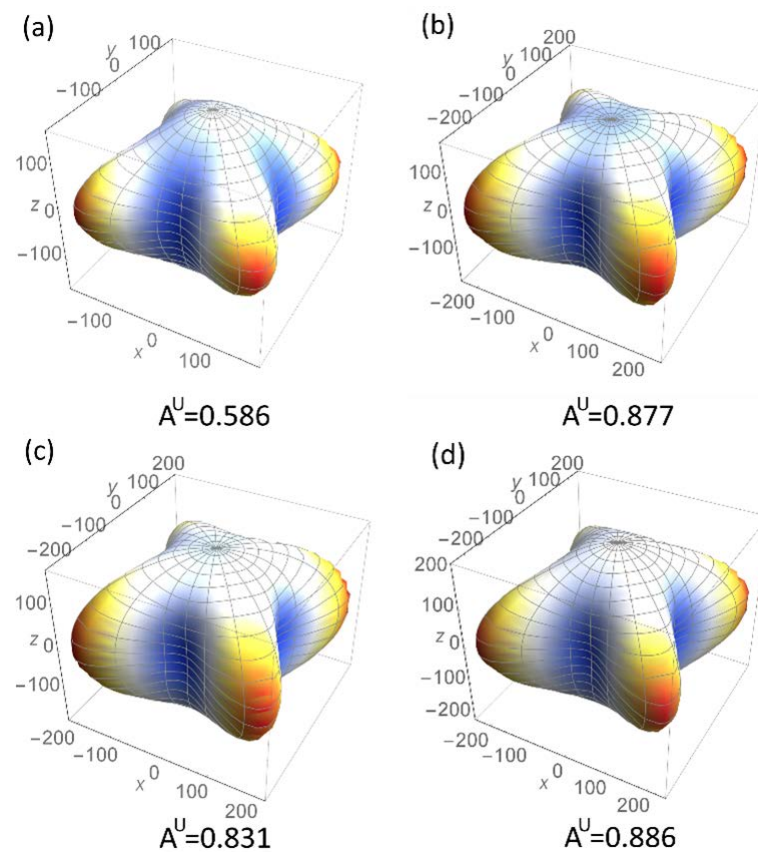


**Figure 1.** The crystal structure of  $U_3Si_2C_2$  (blue: uranium; grey: carbon; yellow: silicon).

**Table 1.** The experimental and calculated values of lattice parameters  $a$ ,  $c$  (Å) and the cell volume ( $\text{Å}^3$ ) of  $U_3Si_2C_2$  calculated by changing  $U$  values.

$U_3Si_2C_2$		$a$ (Å)	$c$ (Å)	$V$ ( $\text{Å}^3$ )
Exp. [30]		3.5735	18.882	241.12
GGA + $U$ ( $U = 4$ eV) [31]		3.672	17.60	237.5
PAW-GGA		3.645	16.790	222.24
GGA + $U$	$U = 1$ eV	3.634	17.372	229.43
	$U = 2$ eV	3.628	17.664	232.55
	$U = 3$ eV	3.639	17.900	237.04
	$U = 3.5$ eV	3.651	18.052	240.58
	$U = 4$ eV	3.705	17.903	245.75

### 3.2. Stability of Ground State Structure

The dynamical stability of  $U_3Si_2C_2$  has been confirmed by phonon dispersion curves and its phonon density of states. As shown in Figure 2, the absence of imaginary frequency appearing in the Brillouin zone demonstrated the structure is dynamically stable at 0 K. C sublattice occupied higher vibration frequency bands in the phonon dispersion, the value of which are in the range of 10.0–12.0 THz and 18.6–20.4 THz. The vibration frequency of phonon dispersion is determined by the relative atomic mass; hence the low vibration frequency bands (below 5 THz) are mainly originated from the vibrations of the metal U sublattice. A maximum peak can be observed at the frequency of 9.03 THz in the phonon density of states (p-DOS) in Figure 2, indicating that the lattice vibration of the  $U_3Si_2C_2$  crystal is mainly concentrated on this frequency.

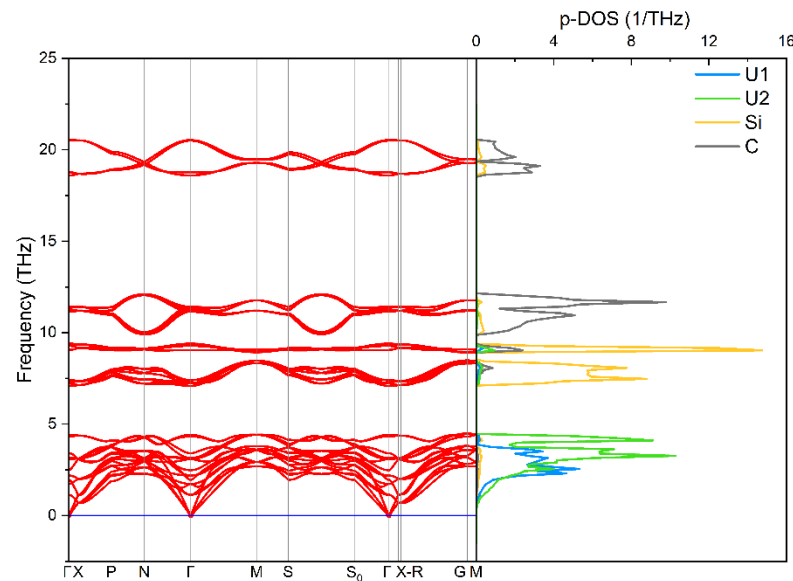


**Figure 2.** The phonon dispersion curves and the phonon density of states (p-DOS) for  $U_3Si_2C_2$ .

The mechanical stability of  $U_3Si_2C_2$  can be judged by elastic constants. For the tetragonal (I) symmetry, there exists six independent elastic constants, namely  $C_{11}$ ,  $C_{12}$ ,  $C_{13}$ ,  $C_{33}$ ,  $C_{44}$ , and  $C_{66}$  [54], and the calculated elastic constants are listed in Table 2. All elastic constants obey the elastic stability criteria list as the Equation (11), proving this specific crystal is mechanically stable.

$$C_{11} > C_{12}2C_{13}^2 < C_{33} \times (C_{11} + C_{12})C_{44} > 0 \quad (11)$$

**Table 2.** Calculated independent elastic constants (all in GPa) of  $U_3Si_2C_2$ .

Compound	$C_{11}$	$C_{12}$	$C_{13}$	$C_{33}$	$C_{44}$	$C_{66}$
$U_3Si_2C_2$	212.268	130.170	61.994	188.622	63.394	108.233

In order to evaluate the thermodynamically stability of  $U_3Si_2C_2$ , the average formation energy ( $\Delta E$ ) has been calculated as the following Equation (12):

$$\Delta E = \frac{1}{N_U + N_{Si} + N_C} [E_{total} - (N_U E_U + N_{Si} E_{Si} + N_C E_C)] \quad (12)$$

where  $E_{total}$  is the total energy of the calculated  $U_3Si_2C_2$  unit cell,  $N_U$ ,  $N_{Si}$ , and  $N_C$  represent the number of atoms in the cell, and  $E_U$ ,  $E_{Si}$ , and  $E_C$  denote the energy of single atom of bulk U (Cmcm), Si (Fd $\bar{3}$ m), and C (R $\bar{3}$ m). In our calculation, the average  $\Delta E$  have a negative value of  $-0.252$  eV/atom, which indicates that the structure shows thermodynamical stability.

Besides, as an important performance metric of nuclear materials, the thermal stability has also been evaluated by Ab initio molecular dynamics (AIMD) simulations over supercells composite of 56 atoms. The simulation with a total duration of 10,000 fs is performed from 300 K to 2200 K with a time step of 1 fs. The peritectic reaction observed at about 1700 °C in the former research [55–57] illustrates that the phase of  $U_3Si_2C_2$  decompose into UC and a liquid phase of composition close to  $USi_2$  by taking the phase diagram into consideration. As shown in Figure 3a, the average energy of  $U_3Si_2C_2$  is almost unchanged below 1973 K, and which emerge a steep drop at the time of 7.0 ps and 5.3 ps in the case of 1973 K and 2200 K. In Figure 3b, the bond length of C-Si stabilizes at 1.9 Å below 1973 K, while the curves rise sharply and oscillate continuously at 1973 K and 2200 K. The curves of energy and bond length indicate that the structure of  $U_3Si_2C_2$  is unstable in the environ-

ment of exceeding 1973 K, reflected in the destruction of the C-Si bond. The instability of C-Si bond above 1973 K can also be illustrated by the absence of the peak at around 1.9 Å in the radial distribution function curves shown in Figure 3c.

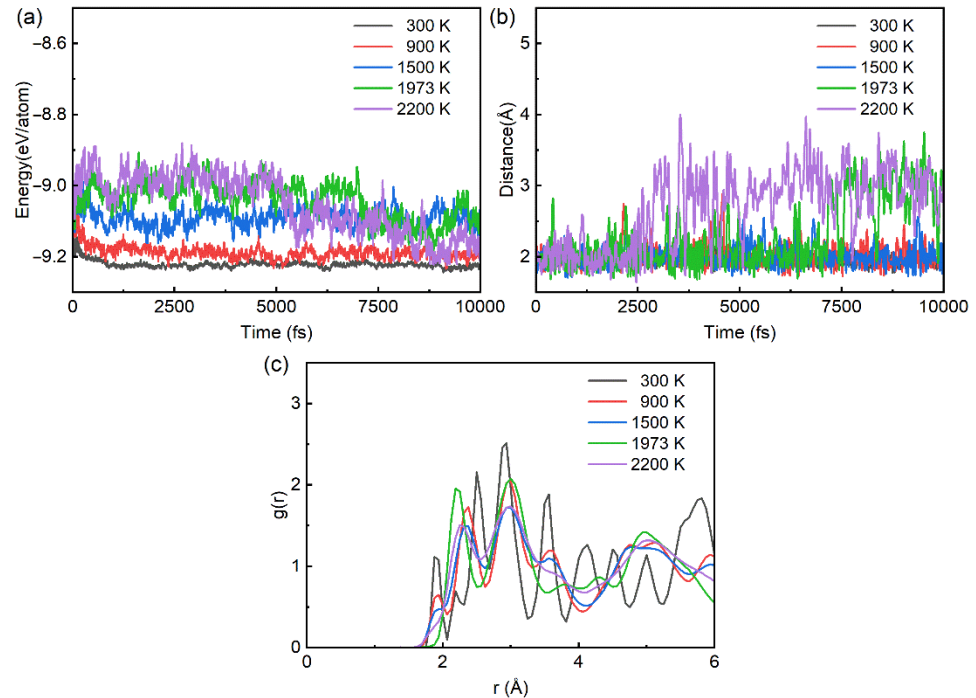
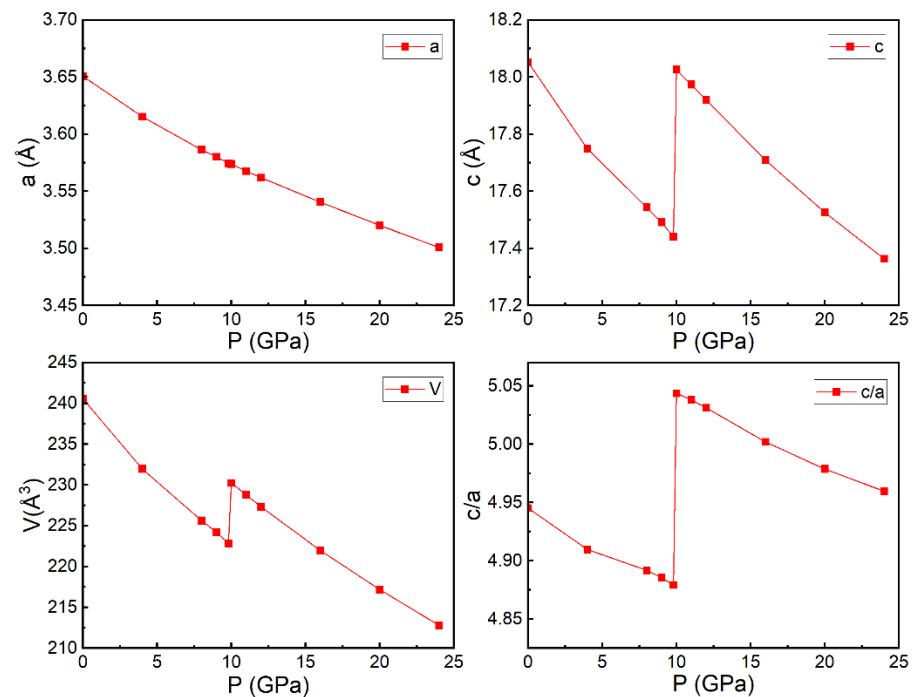


**Figure 3.** The (a) average energy per atom, (b) C–Si distance, and (c) radial distribution function variation during the Ab initio molecular dynamics (AIMD) simulation of  $U_3Si_2C_2$  at 300 K, 900 K, 1500 K, 1973 K, and 2200 K.

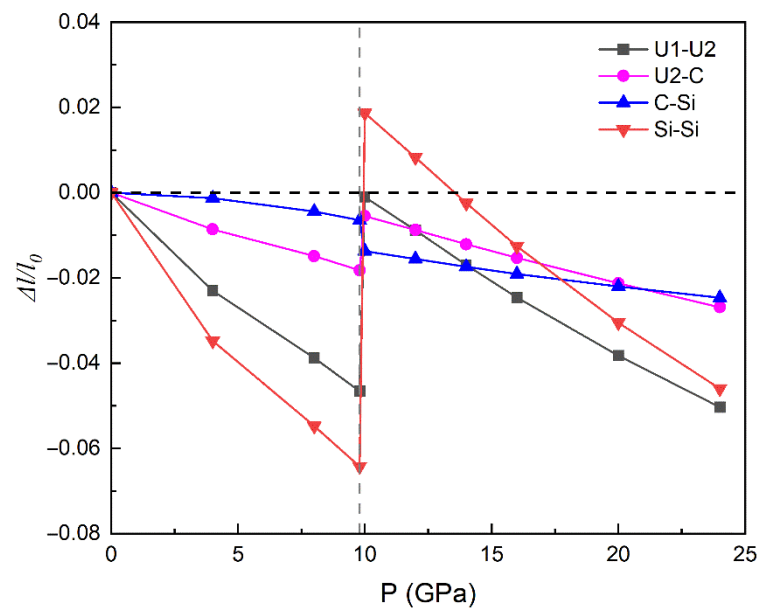
### 3.3. Properties under High Pressure

#### 3.3.1. Structural Parameters and Electronic Behaviors

The structural optimization from 0 GPa to 24 GPa have been carried out by adding isotropic external stress to stress tensor in VASP code [37,38]. The lattice parameters of the optimized cells under different pressures are listed in the supplementary materials (Table S1 and Figure S1). Figure 4 shows the variations of lattice parameters ( $a$  and  $c$ ), cell volume ( $V$ ) and  $c/a$  as a function of pressure. The lattice constants and volumes decrease as the pressure increases at the beginning, moreover, the decrease of lattice parameter  $c$  is faster than that of parameter  $a$ . However, the lattice parameter  $c$  increased dramatically from 17.44 Å to 18.02 Å when the external stress reached 9.8 GPa, resulting in a sudden increase in the cell volume. To explore the mechanism for the increase of lattice parameters, the ratio of the interatomic distance for the U1-U2, U2-C, C-Si, and Si-Si atom pairs along the  $c$  direction under high pressure to that under 0 GPa have been calculated (Figure 5). The value of distance for the Si-C pair decrease slower compared to other atom pairs when the external pressure is below 9.8 GPa. While the external pressure exceeds 9.8 GPa, the Si-C distance reducing by 0.7% shows obviously opposite trend compared to the other atom pairs, which may be explained by the formation of covalent bond between Si and C atoms. When the external pressure reaches 9.8 GPa, the distance of U1-U2 almost changes to the original length (0 GPa), and the Si-Si distance is even 0.058 Å higher. In order to study the sharply variation of  $c$ -axis and volume mutations, the density of states (DOS) under different external pressures, including total density of states (TDOS) and the partial density of states (PDOS) of  $U_3Si_2C_2$ , have been calculated to analyze its electronic structure.



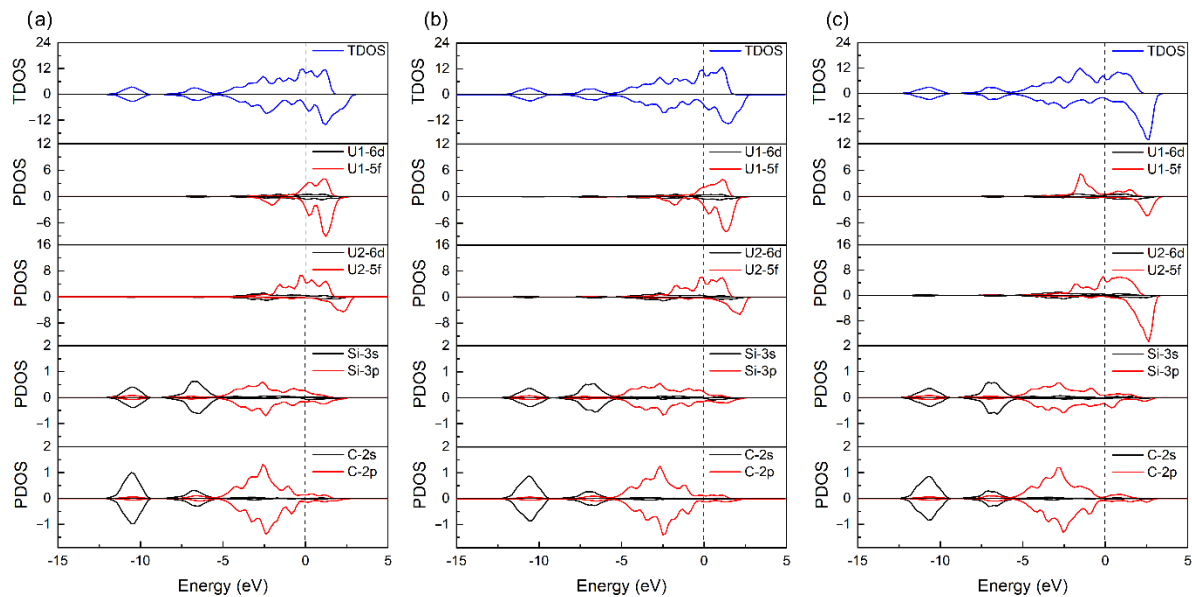
**Figure 4.** Variations of the unit cell parameters  $a$ ,  $c$ , cell volume ( $V$ ) and  $c/a$  as a function of pressure.



**Figure 5.** The variation ratios of interatomic distance for U1-U2, U2-C, C-Si, and Si-Si pairs at  $c$  axis as a function of pressure. The corresponding interatomic distance at 0 GPa ( $l_0$ ) is 3.249, 2.293, 1.922, and 3.122 Å.

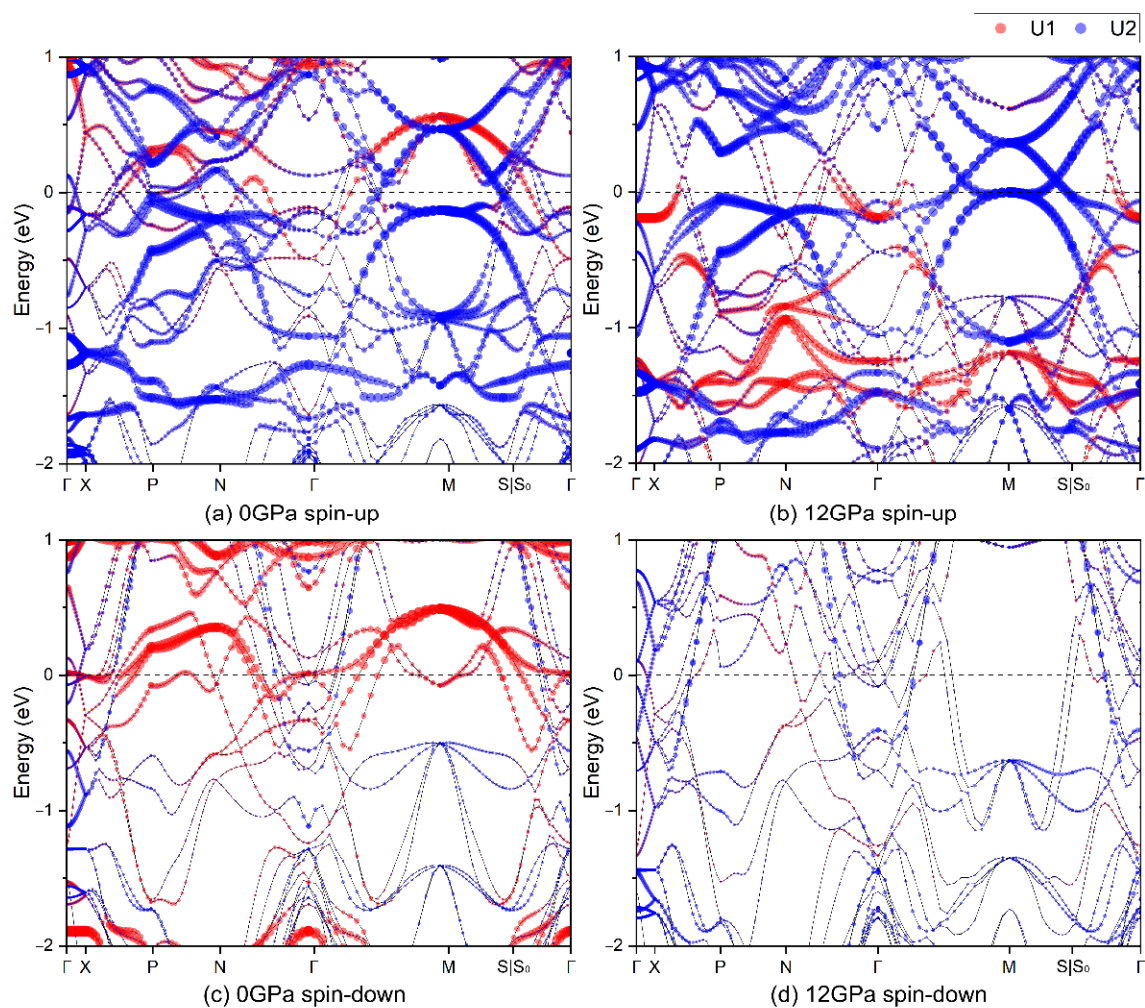
The calculated DOS curves are shown in Figure 6, and more information can be seen in supplementary Figure S2. It can be seen that the state density curves at 0 GPa in Figure 6a pass through the Fermi energy level, indicating  $U_3Si_2C_2$  has metallic properties. The curve for the total density of states displays slight asymmetry, indicating magnetic moment existing in the lattice which is mainly originating from the 5f electrons of uranium atoms (at both U1 and U2 sites) as shown in the partial density of states. Strong interactions between the s orbitals of Si atoms and C atoms can be observed around the peaks at the energy of  $-10.5$  eV and  $-6.7$  eV. The intense peak of 5f states at the Fermi level suggests delocalized nature of uranium 5f electrons. The value of magnetic moments of atoms at U1 and U2

sites are  $-0.61 \mu_B$  and  $2.08 \mu_B$ , respectively. The TDOS and PDOS at 8 GPa vary slightly compared to that at 0 GPa; however, when the pressure increases to 12 GPa, the density of states of U1 atoms near the Fermi level is close to 0, indicating that its metallicity is sharply weakened (showing in Figure 6c). Besides, the spin-down peak of U1-5f orbital in locating at  $-2$  eV disappeared, and a spin-up peak locating at  $-1.6$  eV appeared. Therefore, the magnetic moment of the U1 atom turns positive under the pressure of 12 GPa, and U1 atom has the same direction of magnetic moments as the U2 atom. In conclusion, the c-axis and volume mutation mentioned above may be caused by charge redistributions due to the external pressure, and the specific mechanism and impact will be reported in future work.



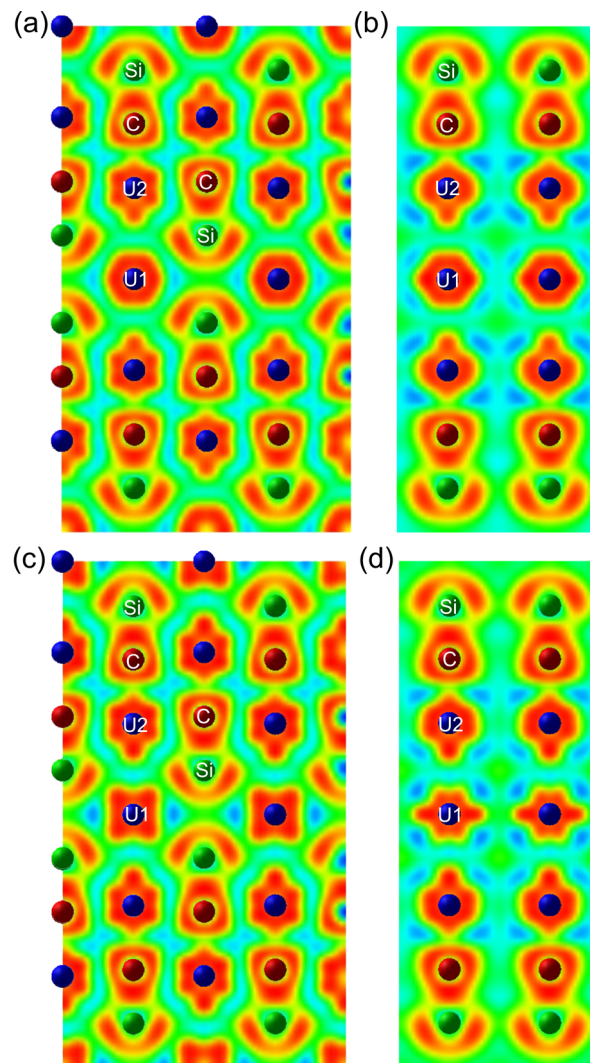
**Figure 6.** The total density of state (TDOS) and partial density of state (PDOS) of  $U_3Si_2C_2$  under different pressures. (a) 0 GPa; (b) 8 GPa; and (c) 12 GPa. The dash line represents Fermi energy.

The projected band-structures of U atoms (divided into U1 site and U2 site) of  $U_3Si_2C_2$  at 0 GPa and 12 GPa have been calculated as shown in Figure 7. With the pressure increasing to 12 GPa, the contribution of uranium atoms around the Fermi level gradually decreases, and the result is consistent with the previous PDOS analysis. Moreover, the contribution around the Fermi level of U1 atoms in the spin-down energy band under 12 GPa significantly reduced compared to U2 atoms. In addition, the band structures at  $\Gamma$  point without external pressure shows that the spin-up electrons have almost no contribution at Fermi surface, while an electron pocket formed by the spin-down electrons which are mainly contributed by the U1 atoms appears. Furthermore, multiple-electron pockets located at Fermi surface formed by spin-up electrons can be observed at  $\Gamma$  point under 12 GPa, which are dominated by both U1 and U2 atoms, while the spin-down electron pocket are mainly contributed by U2 atoms.



**Figure 7.** The spin-up and spin-down band structures of  $U_3Si_2C_2$  at 0 GPa and 12 GPa. The projection on U1 and U2 atoms are included. The dash line represents Fermi surface.

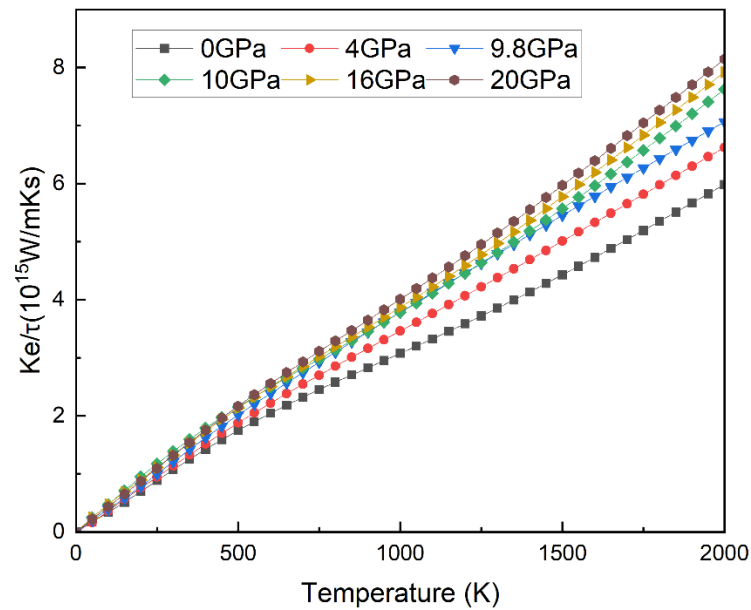
Properties related to electron localization obtained from the electron localization function (ELF) [58] showing in Figure 8 is calculated to reveal atomic bonding of  $U_3Si_2C_2$ . In Figure 8a,b, the formation of C-Si covalent bonds can be revealed that the charge is mainly concentrated between C and Si atoms, and the electrons of Si atoms are more delocalized as to that of C atoms. The distribution of electrons at atomic gaps suggests a metallic behavior of the compound. The crown-shaped charge accumulations between U and Si implies the U–Si bond is biased towards the ionic bond, and similar structure has been reported in  $U_3Si_2$ . In our previous research, the Si-Si bond is covalent in  $U_3Si_2$  [19,20,42], however, no similar Si-Si bond can be observed in  $U_3Si_2C_2$  structure. At the external pressure of 12 GPa, the degree of electronic localization at the U1 site displays more anisotropic, as shown in Figure 8c,d. The differences concerning the charge of  $U_3Si_2C_2$  structure under high pressures may cause some variations on the properties associating with the electronic structure closely, such as thermal conductivity and elastic constants.



**Figure 8.** The electron localization function slice (a) along the [110] plane at 0 GPa; (b) along the [100] plane at 0 GPa; (c) along the [110] plane at 12 GPa; and (d) along the [100] plane at 12 GPa.

### 3.3.2. Thermal and Mechanical Properties

Thermal conductivity is critical to nuclear fuel because it determines the temperature gradients between the surface and centerline of fuel, which may cause thermal stress and make the nuclear fuel deform and generate cracks in the cladding. The electronic thermal conductivity ( $K_e/\tau$ ) is obtained by solving Boltzmann transport equations which can be achieved in BoltzTraP2 [59] as shown in Figure 9. The curves illustrate that the electronic thermal conductivity showed positive correlated with temperature, besides, the applied pressure can also influence the electronic thermal conductivity. However, when the applied pressure is more than 10 GPa, the slope of the curve remains basically unchanged, implying that the applied pressure may not be the major factor to affect the electronic thermal conductivity in the condition that the pressure exceeds 10 GPa.

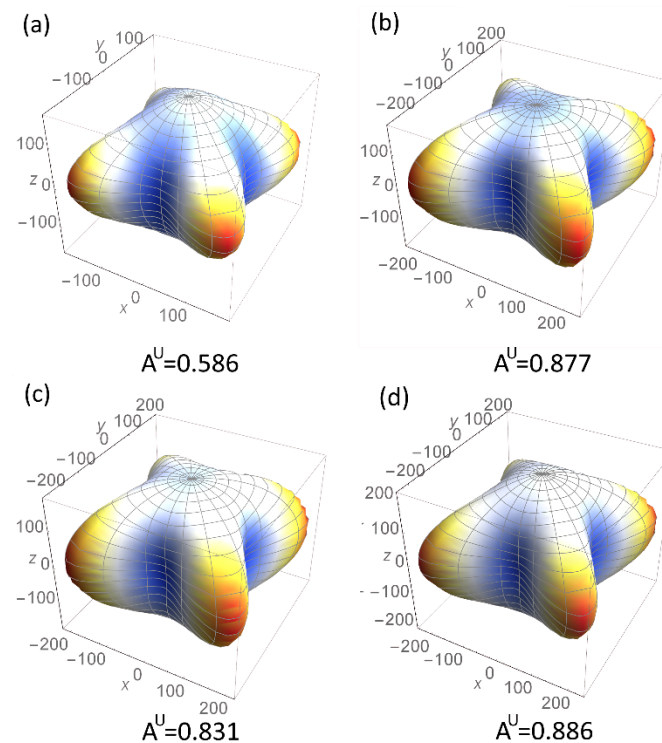


**Figure 9.** The electronic thermal conductivity of  $U_3Si_2C_2$  with dependent relaxation time.

The mechanical anisotropy properties of the nuclear materials may cause the deformation and fractures imposed with external stress. In this work, the mechanical anisotropy is evaluated by universal anisotropic index  $A^U$  and three-dimensional (3D) Young's modulus (E). The universal anisotropic index  $A^U$  is used to evaluate the mechanical anisotropy, which is suitable for describing single crystals of various types [53]. When  $A^U = 0$ , it is shown that the crystal is isotropic, and the difference between its value and 0 can be used to evaluate the degree of anisotropy. The calculated Young's modulus (E), bulk modulus (B), shear modulus (G), and Poisson's ratio under different pressures are also shown in Table 3 to evaluate the mechanical properties of  $U_3Si_2C_2$ . The Poisson's ratio is associated with the properties of interatomic bonding, the value of Poisson's ratio is small ( $\nu = 0.1$ ) for covalent materials, and for ionic crystals it reaches 0.25, whereas for metallic materials it is 0.33 typically [60]. According to the calculated Poisson's ratio, ionic and metallic nature coexist as to the bonding characteristics of  $U_3Si_2C_2$ , moreover, the ionic takes the dominant position in bonding. In our previous research, bonding behaviors of  $U_3Si_2$  ( $\nu = 0.20$ ) [42] is mainly reflected on ionic nature, and  $U_3Si_2C_2$  shows better toughness compared to  $U_3Si_2$ , which may provide theoretical support for the application of  $U_3Si_2C_2$  in nuclear reactors. As the pressure increases to 9.8 GPa, the atomic distance between U1 and U2 decreases from 3.249 Å to 3.098 Å, which may lead to the strength of the metal bond between uranium atoms. When the external pressure applied from 0 GPa to 8 GPa, the Young's modulus, shear modulus and bulk modulus of  $U_3Si_2C_2$  increase 37.8, 34.5 and 14.2 GPa respectively, then decrease sharply as the external pressure exceeds 9.8 GPa, and the changing trend of which seems to be consistent with the variation of the crystal lattice constant. As shown in Figure 10, the three-dimensional Young's modulus distribution of  $U_3Si_2C_2$  at different pressures and the general anisotropy index  $A^U$  indicate that with the increase of hydrostatic pressure, the maximum Young's modulus increases gradually. The maximum Young's modulus of  $U_3Si_2C_2$  under different pressures are all appear along the [110] direction. The maximum value of 3D Young's modulus is 252 GPa under 0 GPa pressure, and raising to 317 GPa, 289.26 GPa, and 319.59 GPa, respectively, under the external pressure 8 GPa, 12 GPa, and 20 GPa. Under high-pressure environment, the value of  $A^U$  for  $U_3Si_2C_2$  increases to higher than 0.8, while that remains basically unchanged when the pressure exceeds 8 GPa. Hence as the pressure increases, the degree of isotropy for  $U_3Si_2C_2$  is reduced slightly.

**Table 3.** Calculated independent elastic constants (all in GPa) of  $U_3Si_2C_2$ .

Pressure (GPa)	E (GPa)	B (GPa)	G (GPa)	$\nu$
0	170.895	122.622	67.402	0.268
8	208.740	157.157	81.626	0.279
12	197.671	141.395	78.008	0.267
20	210.763	162.239	82.106	0.283

**Figure 10.** 3D Young's modulus (E) of  $U_3Si_2C_2$  (unit: GPa) with external pressure of (a) 0 GPa, (b) 8 GPa, (c) 12 GPa, and (d) 20 GPa. The anisotropic index  $A^U$  are presented.

#### 4. Conclusions

In our present research, the structural characteristics, electronic behaviors as well as mechanical properties of  $U_3Si_2C_2$  compounds under high pressure have been calculated. The lattice constants and volumes decrease as the pressure increases; however, the lattice parameter  $c$  increased dramatically when the external stress reached 9.8 GPa, resulting in a sudden increase in the cell volume. U1 and U2 have opposite magnetic moment directions, while the magnetic moment direction of U1 atoms reverse under high pressures. Ionic and metallic nature coexist as to the bonding characteristics of  $U_3Si_2C_2$ , and the ionic takes the dominant position in bonding. The temperature as well as the pressure influences the electronic thermal conductivity of  $U_3Si_2C_2$ , while the electronic thermal conductivity remains basically unchanged with the applied pressure exceeds 10 GPa. Lastly, the maximum value of 3D Young's modulus is 252 GPa under 0 GPa, and the maximum Young's modulus of  $U_3Si_2C_2$  under different pressures are all appear along the [110] direction. Our theoretical investigation may provide support for the application of U-Si-C-based fuels.

**Supplementary Materials:** The following are available online at <https://www.mdpi.com/article/10.3390/cryst11111420/s1>.

**Author Contributions:** M.B., Y.G., and S.D. conceived of the presented idea. M.B. developed the theory and performed the computations. D.S., Y.Y., and Z.L. verified the analytical methods. Y.Y., J.S., Y.L., and E.W. encouraged M.B. to investigate ab initio molecular dynamics and supervised the

findings of this work. E.W., X.C., and Y.Q. participated in discussions. All authors discussed the results and contributed to the final manuscript. All authors have read and agreed to the published version of the manuscript.

**Funding:** The authors acknowledge the financial support of the National Key Research and Development Program of China (No. 2019YFB1901001, 2016YFB0700100), the Zhejiang Province Key Research and Development Program (No. 2019C01060), National Natural Science Foundation of China (Grants No. 21875271, 21707147, 11604346, 21671195, 51872302), Programs Supported by Ningbo Natural Science Foundation (No. 2019A610106), K.C. Wong Education Foundation (rczx0800), the Foundation of State Key Laboratory of Coal Conversion (Grant J18-19-301) the project of the key technology for virtue reactors from NPIC, and the defense industrial technology development program JCKY 2017201C016. We also acknowledge One Thousand Youth Talents Program of China, Hundred-Talent Program of Chinese Academy of Sciences.

**Institutional Review Board Statement:** Not applicable.

**Informed Consent Statement:** Not applicable.

**Data Availability Statement:** The data presented in this study are available in the Supplementary Materials.

**Conflicts of Interest:** The authors declare no conflict of interest.

## References

1. Zinkle, S.J.; Terrani, K.A.; Gehin, J.C.; Ott, L.J.; Snead, L.L. Accident tolerant fuels for LWRs: A perspective. *J. Nucl. Mater.* **2014**, *448*, 374–379. [[CrossRef](#)]
2. Lopes, D.A.; Kocevski, V.; Wilson, T.L.; Moore, E.E.; Besmann, T.M. Stability of U<sub>5</sub>Si<sub>4</sub> phase in U-Si system: Crystal structure prediction and phonon properties using first-principles calculations. *J. Nucl. Mater.* **2018**, *510*, 331–336. [[CrossRef](#)]
3. Ortega, L.H.; Blamer, B.J.; Evans, J.A.; McDeavitt, S.M. Development of an accident-tolerant fuel composite from uranium mononitride (UN) and uranium sesquisilicide (U<sub>3</sub>Si<sub>2</sub>) with increased uranium loading. *J. Nucl. Mater.* **2016**, *471*, 116–121. [[CrossRef](#)]
4. White, J.T.; Nelson, A.T.; Byler, D.D.; Safarik, D.J.; Dunwoody, J.T.; McClellan, K.J. Thermophysical properties of U<sub>3</sub>Si<sub>5</sub> to 1773K. *J. Nucl. Mater.* **2015**, *456*, 442–448. [[CrossRef](#)]
5. White, J.T.; Nelson, A.T.; Byler, D.D.; Valdez, J.A.; McClellan, K.J. Thermophysical properties of U<sub>3</sub>Si to 1150K. *J. Nucl. Mater.* **2014**, *452*, 304–310. [[CrossRef](#)]
6. White, J.T.; Nelson, A.T.; Dunwoody, J.T.; Byler, D.D.; McClellan, K.J. Thermophysical properties of U<sub>3</sub>Si to 1673 K. *J. Nucl. Mater.* **2016**, *471*, 129–135. [[CrossRef](#)]
7. White, J.T.; Nelson, A.T.; Dunwoody, J.T.; Byler, D.D.; Safarik, D.J.; McClellan, K.J. Thermophysical properties of U<sub>3</sub>Si<sub>2</sub> to 1773K. *J. Nucl. Mater.* **2015**, *464*, 275–280. [[CrossRef](#)]
8. White, J.T.; Nelson, A.T.; Dunwoody, J.T.; Safarik, D.J.; McClellan, K.J. Corrigendum to “Thermophysical properties of U<sub>3</sub>Si<sub>2</sub> to 1773 K” [*J. Nucl. Mater.* **2015**, *464*, 275–280]. *J. Nucl. Mater.* **2017**, *484*, 386–387. [[CrossRef](#)]
9. Klipfel, M.; Di Marcello, V.; Schubert, A.; van de Laar, J.; Van Uffelen, P. Towards a multiscale approach for assessing fission product behaviour in UN. *J. Nucl. Mater.* **2013**, *442*, 253–261. [[CrossRef](#)]
10. Frost, B.R.T. The carbides of uranium. *J. Nucl. Mater.* **1963**, *10*, 265–300. [[CrossRef](#)]
11. De Coninck, R.; Van Lierde, W.; Gijs, A. Uranium carbide: Thermal diffusivity, thermal conductivity and spectral emissivity at high temperatures. *J. Nucl. Mater.* **1975**, *57*, 69–76. [[CrossRef](#)]
12. Corradetti, S.; Manzolaro, M.; Andrighetto, A.; Zanonato, P.; Tusseau-Nenez, S. Thermal conductivity and emissivity measurements of uranium carbides. *Nucl. Instrum. Methods Phys. Res. Sect. B Beam Interact. Mater. At.* **2015**, *360*, 46–53. [[CrossRef](#)]
13. Mankad, V.H.; Jha, P.K. Thermodynamic properties of nuclear material uranium carbide using density functional theory. *J. Therm. Anal. Calorim.* **2016**, *124*, 11–20. [[CrossRef](#)]
14. Song, J.; Guo, Y.; Bu, M.; Liu, Z.; Shi, D.; Huang, Q.; Du, S. Theoretical investigations on the U<sub>2</sub>Mo<sub>3</sub>Si<sub>4</sub> compound from first-principles calculations. *Prog. Nucl. Energy* **2020**, *118*, 103121. [[CrossRef](#)]
15. Ugajin, M.; Itoh, A. Experimental investigations on the chemical state of solid fission-product elements in U<sub>3</sub>Si<sub>2</sub>. *J. Alloys Compd.* **1994**, *213–214*, 369–371. [[CrossRef](#)]
16. Ugajin, M.; Itoh, A.; Okayasu, S.; Kazumata, Y. Uranium molybdenum silicide U<sub>3</sub>MoSi<sub>2</sub> and phase equilibria in the U–Mo–Si system. *J. Nucl. Mater.* **1998**, *257*, 145–151. [[CrossRef](#)]
17. Rabin, D.; Shneck, R.Z.; Rafailov, G.; Dahan, I.; Meshi, L.; Brosh, E. Thermodynamic modeling of Al–U–X (X=Si,Zr). *J. Nucl. Mater.* **2015**, *464*, 170–184. [[CrossRef](#)]
18. Chen, X.; Qin, Y.; Shi, D.; Guo, Y.; Song, J.; Bu, M.; Zhang, Y.; Huang, Q.; Liu, G.; Chai, Z.; et al. Investigations of the stability and electronic structures of U<sub>3</sub>Si<sub>2</sub>-Al: A first-principles study. *Chem. Phys.* **2021**, *543*, 111088. [[CrossRef](#)]

19. Chen, X.; Qin, Y.; Shi, D.; Guo, Y.; Bu, M.; Yan, T.; Song, J.; Liu, G.; Zhang, Y.; Du, S. First-principles investigations on the anisotropic elasticity and thermodynamic properties of U<sub>3</sub>Si<sub>2</sub>-Al. *RSC Adv.* **2020**, *10*, 35049–35056. [[CrossRef](#)]
20. Wu, E.; Qiu, N.; Luo, K.; Chen, X.; Shi, D.; Bu, M.; Du, S.; Chai, Z.; Huang, Q.; Zhang, Y. The studies of electronic structure, mechanical properties and ideal fracture behavior of U<sub>3</sub>Si<sub>1.75</sub>Al<sub>0.25</sub>: First-principle investigations. *J. Mater. Res. Technol.* **2021**, *15*, 1356–1369. [[CrossRef](#)]
21. Duan, L.; Gao, R.; Huang, Q.; Jia, J.; Li, B.; Liu, X.; Tang, H.; Wang, Z.; Yang, Z.; Zhong, Y. Preparing Imitated MAX Phase Fault-tolerant Nuclear Fuel Pellet Comprises e.g. Wet Mixing Uranium Dioxide, Silicon-Containing Phase, Carbon Powder, Binder and Sintering Aid Using Ethanol as Wet Mixed Solvent, Mixing, and Processing. China Patent CN106927832, 13 April 2017.
22. Duan, L.; Gao, R.; Huang, Q.; Jia, J.; Li, B.; Liu, X.; Tang, H.; Wang, Z.; Yang, Z.; Zhong, Y.; et al. Uranium-Silicon-Carbon Ternary Compound Fuel Pellet for Preparing Nuclear Fuel, Comprises Uranium-Silicon-Carbon Ternary Compound with Tetragonal Crystal Structure. China Patent CN107082430, 27 May 2017.
23. Garcia, P.; Carlot, G.; Dorado, B.; Maillard, S.; Sabathier, C.; Martin, G.; Oh, J.Y.; Welland, M.J. *Mechanisms of Microstructural Changes of Fuel under Irradiation*; Nuclear Energy Agency of the OECD (NEA): Paris, France, 2015; pp. 24–60.
24. Wang, T.; Li, R.; Quan, Z.; Loc, W.S.; Bassett, W.A.; Xu, H.; Cao, Y.C.; Fang, J.; Wang, Z. Pressure Processing of Nanocube Assemblies Toward Harvesting of a Metastable PbS Phase. *Adv. Mater.* **2015**, *27*, 4544–4549. [[CrossRef](#)] [[PubMed](#)]
25. Lü, X.; Wang, Y.; Stoumpos, C.C.; Hu, Q.; Guo, X.; Chen, H.; Yang, L.; Smith, J.S.; Yang, W.; Zhao, Y.; et al. Enhanced Structural Stability and Photo Responsiveness of CH<sub>3</sub>NH<sub>3</sub>SnI<sub>3</sub> Perovskite via Pressure-Induced Amorphization and Recrystallization. *Adv. Mater.* **2016**, *28*, 8663–8668. [[CrossRef](#)] [[PubMed](#)]
26. Sears, V.F. Neutron scattering lengths and cross sections. *Neutron News* **1992**, *3*, 26–37. [[CrossRef](#)]
27. Smith, G.V.; Smith, R.G.; Thomas, A.G. A Study of the Phase Relationships in the Uranium-Silicon-Carbon System. In Proceedings of the Symposium on Carbides in Nuclear Energy, Harwell, England, 5–7 November 1963; pp. 261–265.
28. Blum, P.L.; Guinet, P.; Silvestre, G. Structure d'une phase nouvelle, U<sub>3</sub>C<sub>3</sub>Si<sub>2</sub>, dans le système uranium-carbone-silicium. *Comptes Rendus Hebd. Des Seances De L Acad. Des Sci.* **1965**, *260*, 1911–1913.
29. Blum, P.L.; Silvestre, G. La structure cristalline du composé U<sub>20</sub>C<sub>3</sub>Si<sub>16</sub>. *Comptes Rendus Hebd. Des Seances De L Acad. Des Sci. Ser. B* **1966**, *263*, 709–711.
30. Pöttgen, R.; Kaczorowski, D.; Jeitschko, W. Crystal structure, magnetic susceptibility and electrical conductivity of the uranium silicide carbides U<sub>3</sub>Si<sub>2</sub>C<sub>2</sub> and U<sub>20</sub>Si<sub>16</sub>C<sub>3</sub>. *J. Mater. Chem.* **1993**, *3*, 253–258. [[CrossRef](#)]
31. Matar, S.F.; Pöttgen, R. First principles investigations of the electronic structure and chemical bonding of U<sub>3</sub>Si<sub>2</sub>C<sub>2</sub>—A uranium silicide-carbide with the rare [SiC] unit. *Chem. Phys. Lett.* **2012**, *550*, 88–93. [[CrossRef](#)]
32. Sahoo, B.D.; Joshi, K.D.; Kaushik, T.C. Structural stability of uranium carbide (UC) under high pressure: Ab-initio study. *Comput. Condens. Matter* **2019**, *21*, e00431. [[CrossRef](#)]
33. Staun Olsen, J.; Gerward, L.; Benedict, U.; Itié, J.P.; Richter, K. High-pressure structural studies of UC by v-ray diffraction and synchrotron radiation. *J. Less Common Met.* **1986**, *121*, 445–453. [[CrossRef](#)]
34. Sahoo, B.D.; Mukherjee, D.; Joshi, K.D.; Kaushik, T.C. High pressure behaviour of uranium dicarbide (UC<sub>2</sub>): Ab-initio study. *J. Appl. Phys.* **2016**, *120*, 085902. [[CrossRef](#)]
35. Guo, X.; Lü, X.; White, J.T.; Benmore, C.J.; Nelson, A.T.; Roback, R.C.; Xu, H. Bulk moduli and high pressure crystal structure of U<sub>3</sub>Si<sub>2</sub>. *J. Nucl. Mater.* **2019**, *523*, 135–142. [[CrossRef](#)]
36. Baker, J.L.; Wang, G.; Ulrich, T.; White, J.T.; Batista, E.R.; Yang, P.; Roback, R.C.; Park, C.; Xu, H. High-pressure structural behavior and elastic properties of U<sub>3</sub>Si<sub>5</sub>: A combined synchrotron XRD and DFT study. *J. Nucl. Mater.* **2020**, *540*, 152373. [[CrossRef](#)]
37. Kresse, G.; Joubert, D. From ultrasoft pseudopotentials to the projector augmented-wave method. *Phys. Rev. B* **1999**, *59*, 1758–1775. [[CrossRef](#)]
38. Kresse, G.; Furthmüller, J. Efficient iterative schemes for ab initio total-energy calculations using a plane-wave basis set. *Phys. Rev. B* **1996**, *54*, 11169–11186. [[CrossRef](#)] [[PubMed](#)]
39. Blöchl, P.E. Projector augmented-wave method. *Phys. Rev. B* **1994**, *50*, 17953–17979. [[CrossRef](#)]
40. Perdew, J.P.; Burke, K.; Ernzerhof, M. Generalized Gradient Approximation Made Simple. *Phys. Rev. Lett.* **1996**, *77*, 3865–3868. [[CrossRef](#)]
41. Dudarev, S.L.; Botton, G.A.; Savrasov, S.Y.; Humphreys, C.J.; Sutton, A.P. Electron-energy-loss spectra and the structural stability of nickel oxide: An LSDA+U study. *Phys. Rev. B* **1998**, *57*, 1505–1509. [[CrossRef](#)]
42. Wang, T.; Qiu, N.; Wen, X.; Tian, Y.; He, J.; Luo, K.; Zha, X.; Zhou, Y.; Huang, Q.; Lang, J.; et al. First-principles investigations on the electronic structures of U<sub>3</sub>Si<sub>2</sub>. *J. Nucl. Mater.* **2016**, *469*, 194–199. [[CrossRef](#)]
43. Monkhorst, H.J.; Pack, J.D. Special points for Brillouin-zone integrations. *Phys. Rev. B* **1976**, *13*, 5188–5192. [[CrossRef](#)]
44. Press, W.H.; Vetterling, W.T.; Teukolsky, S.A.; Flannery, B.P. *Numerical Recipes*; Cambridge University Press: Cambridge, UK, 1986; Volume 818.
45. Giannozzi, P.; de Gironcoli, S.; Pavone, P.; Baroni, S. Ab initio calculation of phonon dispersions in semiconductors. *Phys. Rev. B* **1991**, *43*, 7231–7242. [[CrossRef](#)]
46. Gonze, X.; Lee, C. Dynamical matrices, Born effective charges, dielectric permittivity tensors, and interatomic force constants from density-functional perturbation theory. *Phys. Rev. B* **1997**, *55*, 10355–10368. [[CrossRef](#)]
47. Togo, A.; Tanaka, I. First principles phonon calculations in materials science. *Scr. Mater.* **2015**, *108*, 1–5. [[CrossRef](#)]
48. Ranganathan, S.I.; Ostojica-Starzewski, M. Universal Elastic Anisotropy Index. *Phys. Rev. Lett.* **2008**, *101*, 055504. [[CrossRef](#)]

49. Hill, R. The Elastic Behaviour of a Crystalline Aggregate. *Proc. Phys. Society. Sect. A* **1952**, *65*, 349–354. [[CrossRef](#)]
50. Reuss, A. Berechnung der Fließgrenze von Mischkristallen auf Grund der Plastizitätsbedingung für Einkristalle. *Z. angew. Math. Mech.* **1929**, *9*, 49–58. [[CrossRef](#)]
51. Voigt, W. A determination of the elastic constants for beta-quartz lehrbuch de kristallphysik. *Terubner Leipz.* **1928**, *40*, 2856–2860.
52. Dorado, B.; Freyss, M.; Martin, G. GGA+U study of the incorporation of iodine in uranium dioxide. *Eur. Phys. J. B* **2009**, *69*, 203–209. [[CrossRef](#)]
53. Obodo, K.O.; Chetty, N. GGA+U studies of the early actinide mononitrides and dinitrides. *J. Nucl. Mater.* **2013**, *442*, 235–244. [[CrossRef](#)]
54. Mouhat, F.; Coudert, F.-X. Necessary and sufficient elastic stability conditions in various crystal systems. *Phys. Rev. B* **2014**, *90*, 224104. [[CrossRef](#)]
55. Guinet, P.; Vaugoyeau, H.; Laugier, J.; Blum, P.L. Etude d'un equilibre a 4 phases solides dans le systeme ternaire U-C-Si. *J. Nucl. Mater.* **1967**, *21*, 21–31. [[CrossRef](#)]
56. Rogl, P.; Nol, H. The C-Si-U system (carbon-silicon-uranium). *J. Phase Equilibria* **1995**, *16*, 66–72. [[CrossRef](#)]
57. Guéneau, C.; Sundman, B.; Dupin, N. *Thermodynamic Modelling of the U-Pu-Si-C System*; European Commission: Brussels, Belgium.
58. Becke, A.D.; Edgecombe, K.E. A simple measure of electron localization in atomic and molecular systems. *J. Chem. Phys.* **1990**, *92*, 5397–5403. [[CrossRef](#)]
59. Madsen, G.K.H.; Singh, D.J. BoltzTraP. A code for calculating band-structure dependent quantities. *Comput. Phys. Commun.* **2006**, *175*, 67–71. [[CrossRef](#)]
60. Haines, J.; Léger, J.M.; Bocquillon, G. Synthesis and Design of Superhard Materials. *Annu. Rev. Mater. Res.* **2001**, *31*, 1–23. [[CrossRef](#)]